Light funneling from a photonic crystal laser cavity to an optical nano-antenna: toward antenna-based laser nano-emission

Mathieu Mivelle,†* Pierre Viktorovitch,‡ Fadi I. Baida,† Ali El Eter,† Zhihua Xie,† Than-Phong Vo,‡ Elie Atie,$† Geoffrey W. Burr,¶ Dusan Nedeljkovic,§ Jean-Yves. Rauch,† Ségolène Callard,‡ and Thierry Grosjean,†**

† University of Franche-Comté, FEMTO -ST Institute, UMR CNRS 6174, Besançon, France
‡ University of Lyon, Institute of nanotechnology of Lyon, INL-UMR 5270, CNRS, Ecole Centrale de Lyon, France
$ Department of Physics, University of Balamand, Lebanon
¶ IBM Research - Almaden, San Jose, California 95120, USA
§ Lovalite s.a.s., 18 rue Alain Savary, 25000 Besançon, France

* Current address: ICFO-Institut de Ciencies Fotoniques, Mediterranean Technology Park, 08860 Castelldefels, Barcelona, Spain
** E-mail: thierry.grosjean@univ-fcomte.fr,
Phone: +33 (0)3 81 66 64 17. Fax: +33 (0)3 81 66 64 23

ABSTRACT

We show that the near-field coupling between a photonic crystal microlaser and a nanoantenna can enable hybrid photonic systems that are both physically compact and highly efficient at transferring optical energy into the nano-antenna. Up to 19.4% of the laser power from a micron-scale photonic crystal laser cavity is experimentally transferred to a bowtie aperture nano-antenna (BNA) whose area is 400-fold smaller than the overall emission area of the microlaser. Instead of a direct deposition of the nano-antenna onto the photonic crystal, it is fabricated at the apex of a fiber tip to be accurately placed in the near-field volume of the microlaser. Such light funneling within a hybrid structure provides a path for overcoming the diffraction limit in optical energy transfer to the nanoscale and should thus open promising avenues in the nanoscale enhancement and confinement of light in compact architectures, impacting applications such as biosensing, optical trapping, heating, spectroscopy, and nanoimaging.

Keywords: Nano-antennas, photonic crystal cavities, microlasers, optical funneling, plasmonic-photonic hybrid structure

INTRODUCTION

Optical nano-antennas have attracted intense research interest in the past years due to their unique ability to enhance and confine optical energy down to the nanoscale [1]. One of the main achievements in the development of nano-antennas has been the exploitation of the strong optical electric field produced within the small gap between two coupled metal nanoparticles [2–8]. Such an effect has opened new avenues in the investigation of light-matter interaction at the nanoscale by enhancing locally inherently weak physical processes, such as fluorescence [9-11] and Raman scattering of single molecules [12,13], nonlinear phenomena [14] and optical forces [15].

Nano-antennas are however restricted, both in coupling efficiency and compactness, to being excited by diffraction limited far-field optical waves generated by macroscopic laser sources, and it remains a key fundamental challenge to realize efficient light coupling in nano-antennas from compact laser sources (on the micron size). A way of addressing this issue is to deposit a nano-antenna directly at the end facet of a laser diode [16], but so far the size discrepancy between the diffraction limited emission area of the laser diode and the tightly localized plasmon modes of nano-antennas strongly limits the light coupling in the nano-antenna. The recent achievement of laser emission with Photonic Crystals

(PC) [17–20] introduces the prospect of a direct near-field coupling between a nano-antenna and a microlaser, and thus new hybrid plasmonic/photonic approaches can be imagined to overcome the diffraction limit in nano-antenna addressing. Recent works have predicted that the near-field interaction between plasmonic nano-antennas and PC passive cavities [21–24] can significantly enhance the light coupling efficiency into the nano-antenna. However, these passive hybrid structures are still addressed optically with macroscopic external sources.

In this letter, we use the hybrid plasmonic/photonic approach to show experimentally that up to 19.4 ± 8.1% of the light emitted by a PC microlaser is funneled into a bowtie aperture nano-antenna (BNA) [8] whose area is 400 fold smaller than the overall emission area of the PC microlaser. Given the resonance properties of the BNA [25] the energy is mainly located in the nanometer-size gap region of the nano-antenna. This optical funneling effect relies upon the near-field coupling between two optical resonators of strongly unbalanced quality factors. The laser microcavity (the micro-resonator of high quality factor (Q-factor)) plays the role of a micron-size light accumulator for the nano-antenna, and the nano-antenna (a nano-resonator of low Q-factor) acts as a nanoscale loss channel for the laser microcavity, confined in a volume far below the diffraction limit. This new approach overcomes the diffraction limit in nano-antenna addressing, and thus significant light insertion into a nano-antenna becomes possible in a very compact architecture which does not exceed a few cubic microns. Fabricating a nano-antenna on top of a PC microlaser remains a challenge owing to the positioning exigencies of the nanoantenna to reach optimal performances. We propose here an alternative approach in which the nano-antenna is fabricated at the end of a fiber tip and accurately positioned in the near-field of a PC structure. This way of hybridization provides a unique possibility to study the microlaser-to-nanoantenna optical coupling without intermediate processes of the PC to deposit the nano-antenna. This excludes the risks of changes of the intrinsic optical properties of the PC after nano-antenna fabrication process. The choice of a BNA is motivated by its unique ability to cancel the background excitation signal in its resonance process [26]: the signal collected through the fiber tip is only due to the BNA resonance and direct emission of the microlaser in free space is filtered out. Therefore, the BNA on a fiber tip provides an ideal tool to probe the resonance of the nano-antenna immersed within the near-field of the PC laser nanocavity (without the need of the detection of non-linear processes), and thus it gives detailed information onto its coupling process with the PC laser cavity. Coupling a plasmonic nano-antenna to a laser micro/nano-cavity may thus open promising perspectives in the generation of very high intensities in nanoscale volumes with very compact optical benches and modest energy consumption.

MATERIALS AND METHODS

BNA-on-tip

The fabrication process of the BNA-on-tips is divided in three steps. First, 30μm-long polymer tips are produced at the end of a single mode optical fiber (SMF-28) by a photopolymerization technique [27]. A 100 nm thick aluminum film is then deposited onto the dielectric tip using a thermal vapor deposition technique. Prior to that operation, a 5 nm thick titanium coating is deposited onto the tip to ensure a good adhesion between the polymer and aluminum. Finally, the BNA is fabricated at the very tip by focused ion beam milling. Scanning electron micrographs of a resulting tip-integrated nanostructure are reported in Figures 1(a) and (b).

Figure 1 (a,b) SEM micrographs of the BNA-on-tip: (a) side view and (b) top view of the tip apex. (c): theoretical resonance spectrum of the BNA-on-tip, positioned at a distance of 2 nm beneath an air/InP interface. The excitation plane-wave is incident in the InP substrate and is linearly polarized along the polarization axis of the BNA (ie. the symmetry axis of the BNA that passes through each metal triangle's tip, see the white arrow shown in the figure inset). (d,e) Simulation of the enhancement of optical electric intensity plotted in the transverse plane taken at half the thickness of the metal layer right at the feed gap of the BNA (λ = 1.59μm), for two perpendicular polarization directions of the incoming wave (see arrows).

The BNA's width and gap size are set to 210 nm and 40 nm, respectively, so that the resonance spectrum of the nanostructure is centered at a wavelength of 1590 nm when the tip is close to an InP surface. The design procedure is realized with a 3D Finite Difference Time Domain (FDTD) method [28] which includes a Drude model to define the permittivity of aluminum. Figure 1 (c) displays the resonance spectrum of the BNA-on-tip positioned at a distance of 2 nm from an InP surface (cf. figure inset). The BNA is excited with an incoming plane wave in the InP substrate (at normal incidence from the InP/air interface). This wave is polarized along the symmetry axis of the BNA that passes through each metal triangle's tip (called polarization axis of the BNA in the following, see the white arrow of the figure inset) and it is described by a single temporal pulse. The time-varying optical electric field is calculated at a single grid cell at the center of the nano-antenna feed gap. The spectral response of the system is then obtained with a Fourier-transform of this result and it is normalized by the spectrum calculated with the same procedure without the metallic structure. We see that the BNA resonance is sufficiently broad (Q~3) to ensure high optical field enhancement in its gap zone over a spectral range from 1450 nm to 1650 nm

Figure 1(d,e) show the enhancement of the electric intensity due to the presence of the BNA at 2 nm beneath the InP/air interface, and at λ=1590 nm. These enhancements are the field intensities diffracted by the BNA at a given plane normalized to the intensities calculated at the same plane without the presence of the tip. Intensity plots are simulated along the transverse (XY)-plane which crosses the very tip at half the thickness of the metal layer, for an incident polarization (d) parallel and (e) perpendicular to the polarization axis of the nanostructure. We see that the resonant mode of the BNA, shown in Figure 1(d), is strongly bound to its nanometer-scale feed gap. The electric field enhancement is induced by a resonant optical capacitive effect in between the two closely spaced metal triangles of the BNA, which leads to a charge distribution in the gap zone corresponding to an oscillating electric dipole [25,26]. The dipolar properties of the BNA, which are common to all gap-based nano-antennas, associates the generation of a tiny "hot spot" to a high sensitivity of the nanostructure to the polarization [4,6,29,30]: the tight optical confinement is canceled and the intensity maximum over the antenna is greatly reduced when the BNA is immersed within a field polarized perpendicularly to its polarization axis (see Figure 3 (e)). Therefore, experimental evidence of the polarization sensitivity of a BNA proves that its feed gap produces a highly localized and enhanced electric field upon resonance of the overall nanostructure, as shown for example in Refs. [30,31].

Photonic crystal laser cavity

This BNA-on-tip is coupled to a PC laser nanocavity which consists of a linear defect of 7 air cylindrical holes in a 2D triangular lattice PC [32] (period of 460 nm and hole radius of 100 nm, see Figure 2(b)). The two holes on both edges of the nanocavity are shifted by 80 nm outward in order to increase the Q-factor of the structure by 60 % and thus achieve easier laser emission. The PC microlaser is fabricated into a 250-nm thick InP layer at the center of which are grown four InAsP quantum wells, separated by InP barrier layers. The photoluminescence from the quantum wells occurs between 1450 nm and 1650 nm. The heterostructure is bonded on the top of a transparent SiO_2 substrate which allows optical pumping from the backside and dissipates the heat production during laser emission. The PC is fabricated using e-beam lithography and reactive ion etching. Simulation of the optical properties of this nanocavity with 3D-FDTD method reveals that the structure sustains several optical modes of various Q-factors. The laser emission is however often achieved only with the fundamental mode whose Q-factor (predicted to value of 5800) is large enough to trigger population inversion within the active zone. The structure is designed so that its fundamental mode is resonant at λ =1590 nm. The theoretical distribution of the electric intensity of the fundamental mode is plotted in Figure 2(c-e). Figure 2(c) reports the total simulated electric intensity taken 450 nm beneath the structure and Figure 2(d,e) display the intensity of the electric field components (d) parallel ($|E_x|^2$) and (e) perpendicular ($|E_y|^2$) to the long axis of the nanocavity (oriented along (0x) axis).

Experimental set-up

The experimental set-up developed in the frame of this study is shown in Figure 2(a). The PC microlaser is pumped optically with a pulsed laser beam at λ =780 nm (pulse width of 10 ns with a 5% cyclic ratio) and laser emission occurs at both sides of the InP layer. The pump beam is focused on the structure with a long working distance objective (×60, NA=0.7) that leads to a spot size of about 3 microns. The BNA-on-tip is mounted onto a commercial SNOM from NT-MDT to be positioned in the near-field of the PC. Two detection channels are then implemented. In the first case, the near-field optical signal is collected locally by the BNA-on-tip and guided by the fiber to an InGaAs detector whereas in the second case it is collected with the objective used to focus the pump laser beam onto the PC structure and projected either onto a second InGaAs detector or an optical spectrum analyser. The pump beam is filtered out and a synchronous detection scheme is used to enhance the signal-to-noise ratio in the detection channels involving InGaAs detectors.

Figure 2: (a) Scheme of the experimental set-up. (b) SEM micrograph of the PC nanocavity. (c-e) FDTD simulation of the fundamental mode of the structure at λ=1590 nm: (c) total intensity distribution of the electric field, (d) intensity of the electric field component parallel to the long axis of the nanocavity, ie. the axis of the linear hole defect ($|E_x|^2$), (e) intensity of the electric field component perpendicular to the long axis of the nanocavity ($|E_y|^2$). (f,g) Near-field images of the PC laser nanocavity by the BNA-on-tip used in collection mode (BNA-to-PC spacing about 450 nm): 2D mappings of the resonance of the BNA immersed within the cavity mode. The polarization axis of the BNA is (f) parallel and (g) perpendicular to the cavity long axis (see figure inset). (scalebars: 1590 nm).

RESULTS AND DISCUSSIONS

Figure 2(f,g) report the images accumulated by the BNA-on-tip during the scan of the PC at a constant height of 450 nm, for two orthogonal orientations of the BNA. At this distance, the coupling rate between the two structures is small. The good agreement between Figure 2(f,g) and Figure 2(d,e) shows that the laser emission is due to the excitation of the fundamental mode of the nanocavity. By comparing Figure 2(d) and (f) (Figure 2(e) and (g), respectively), we see that the BNA oriented along (0x) axis (along (0y) axis, respectively) collects selectively the information carried by $|E_x|^2$ ($|E_y|^2$, respectively). Such a polarization sensitivity (measured experimentally to a value of 1:300 in intensity) unambiguously proves that the local collection process is driven by the optical capacitive effect that is resonantly excited within the nanometer scale feed gap of the BNA [25,26]. Since the signal collected by the BNA-on-tip is exclusively due to a resonant transmission phenomenon through the BNA, the images shown in Figure 2(f,g) can be seen as 2D maps of the BNA resonance within the near-field of the PC laser nanocavity. These images thus reveal the near-field coupling between micron size laser mode and the nanoscale resonant mode of the nano-antenna. Note that BNA-on-tips have been proposed as high resolution polarizing nanoprobes for scanning near-field optical microscopy [26,33]. The sample-to-BNA coupling has however not been investigated in these studies.

Figure 3(a) and (b) show the evolution of the emission spectrum of the PC laser nanocavity when the BNA oriented (a) perpendicular and (b) parallel to the nanocavity long axis approaches the surface of the microlaser. In both cases, the BNA-on-tip is centered with respect to the nanocavity and the distance (Z) between the BNA and the nanocavity is given for each spectrum. When the BNA is oriented along (0y), i.e. perpendicularly to the cavity long axis, it is resonantly excited (see the bright spot at the center of Figure 2(f)). For the orthogonal orientation along (0x), the BNA is non-resonant (the center of Figure 2(e) is dark). The recorded signal is the back-radiated laser emission collected by the objective used to focus the pump signal and projected on a spectrophotometer whose spectral resolution is 0.03 nm. The emission peak of the unperturbed PC laser nanocavity, achieved for the larger Z-distances in both figures, is centered at the wavelength λ =1592.7 nm. We see from Figure 3(a,b) that the emission line of the PC laser nanocavity is blueshifted and broadened when the BNA-on-tip approaches the surface of the structure, regardless of the BNA orientation. However, the laser

line broadening (corresponding to an increase of the optical losses) is higher and the spectral blueshift is smaller when the BNA is resonant. Moreover, we note a critical spacing for which the laser emission is quenched, ie. when the Q-factor of the entire device (the PC and the BNA-on-tip) becomes too small to preserve population inversion within the gain medium of the microlaser. This critical distance is about 145 nm when the BNA is resonantly excited (Figure 3(b)) and 95 nm otherwise (Figure 3(a)).

Figure 3: (a,b) Emission spectra of the PC laser nanocavity coupled to a BNA-on-tip whose polarization axis is (a) parallel and (b) perpendicular to the long axis of the PC nanocavity (see figure insets), for various spacings (Z) between the tip apex and the nanocavity. (c) Emission wavelength of the PC laser nanocavity coupled to a BNA-on-tip, as a function of Z. BNA's polarization axis is oriented parallel (blue circles) and perpendicular (red squares) to the cavity long axis (see figure inset). (d) laser linewidth as a function of Z. BNA's polarization axis is oriented parallel (blue circles) and perpendicular (red squares) to the cavity long axis (0*x*) (see figure inset).

Figure 3(c) displays the emission wavelength of the hybrid photonic/plasmonic device as a function of the spacing (Z) between the BNA and the PC laser nanocavity. For $Z > 350$ nm, the perturbation of the nanocavity by the tip is small and the two approach curves recorded for the two BNA perpendicular orientations are similar. For smaller distances, the two curves split and show exponential-like behaviors with respect to the distance *Z*. When the BNA is non resonant (blue circles of Figure 3(c)), we observe mainly the effect of the metal-coated tip which blueshifts the laser emission line. The metal-coated tip placed in the vicinity of the cavity prevents the cavity mode from occupying its overall volume, resulting in a blueshift of the laser emission [34]. When the BNA is resonantly excited (red squares of Figure 3(c)), a smaller blueshift of the laser emission is observed. This lower spectral shift observed when the BNA is resonantly excited shows that the BNA resonance (see Figure 1) and the overall metal-coated tip which holds the BNA have opposite effects onto the microlaser emission wavelength, ie. the BNA resonance redshifts the emission line. The BNA has however a lower impact onto the PC laser nanocavity than the tip since the laser emission keeps blueshifted even if the BNA is resonant. A simple way to filter out the undesirable influence of the tip, and therefore to extract from our experimental data the information about the coupling between the PC and the BNA resonances, is to consider the difference between the two spectral approach curves. Since the tip is the same in the two sets of measurements taken with a BNA on- and off-resonance, this difference represents the spectral shift of the laser emission due to the capacitive effect resonantly excited within the BNA. Ref. [21] shows that a metallic nano-antenna that is non-resonantly excited by a PC nanocavity mode has almost no influence onto the PC resonance properties. Following this procedure, the spectral redshift induced by the BNA resonance is found to be of 0.9 nm at Z=145 nm, ie. around laser threshold when the BNA is resonantly excited.

Figure 3(d) shows the laser linewidth of the hybrid photonic/plasmonic device (noted $\Delta\lambda$) as a function of the spacing Z between the BNA and the PC cavity. The BNA is positioned at the center of the cavity and its polarization axis is set perpendicular (red squares) and parallel (blue circles) to the cavity long axis. Here again, the two approach curves recorded for the two BNA orientations overlap each other for Z values larger than 350 nm. When the BNA is resonantly excited (red squares), the laser linewidth is increased to about 1.7 nm when Z is equal to 150 nm, ie. just above the laser threshold. At the same distance, the laser linewidth is only about 1 nm when the BNA is non resonant (blue circles) and it increases to 1.55 nm when Z is equal to 95 nm. Therefore, the BNA resonance increases the losses within the laser cavity but it has a modest impact onto the microlaser as compared to the overall tip. Following a similar procedure as described above, the undesirable effect of the tip can be filtered out by considering the difference between the two curves. We find that the resulting broadening of the laser linewidth due to the coupling between the BNA and PC resonances is of 0.7 nm, when Z=150 nm.

The laser line broadening induced by the BNA (see inset of Figure 3(d)) is demonstrated to be driven by its resonant capacitive effect by using the laser emission threshold to probe the energy transfer between the photonic and the plasmonic structures. To this end, the BNA-on-tip is placed at a distance

Z=100 nm away from the PC surface so that the laser emission threshold is closely approached when the BNA is not resonantly excited. In that case, any over-added optical loss induced by the BNA resonant mode can trigger laser quenching, and thus the origin of the power transfer from the PC to the BNA can be characterized by analyzing the spatial distribution of laser extinction in the near-field images. The two images shown in Figure 4(a) and (b) are formed simultaneously by raster scanning the BNA across the PC nanocavity at a constant height of 100 nm while detecting the optical signals both transmitted through the BNA into the tip body and radiated from the backside of the PC structure, respectively. The BNA's polarization axis is oriented perpendicularly to the cavity long axis, ie. along (0*y*) (see inset of Figure 4(a)). In the first case (Figure 4(a)), the signal is collected and guided towards a InGaAs detector through the fiber tip (same procedure as detailed previously) whereas in the second case (Figure 4(b)) it is collected and projected onto a second InGaAs detector with the objective used to focus the pump laser beam onto the PC structure. To ensure a satisfying signal-to-noise ratio, a conventional synchronous detection is implemented for each detection channel. Here again, the pump beam is filtered out before detection and no tip-to-sample distance control is required. On the one hand, Figure 4(a) represents a 2D map of the resonance of the BNA immersed within the near-field of the PC nanocavity and is directly comparable to Figure 2(f). On the other hand, Figure 4(b) relates the laser emission power to the position of the BNA with respect to the nanocavity.

Figure 4: (a,b) Near-field mappings of the PC cavity mode when a BNA-on-tip is raster scanned the PC surface: (a) signal collected by the tip and (b) signal collected by the objective used to focus the pump beam onto the PC. The two images are recorded simultaneously while the BNA-on-tip, oriented along (0*y*) (inset of (a)), is raster scanned across the PC structure at a constant height of 100 nm. (b) is a measure of the back-radiated laser power as a function of the tip position with respect to the nanocavity. (c) color-coded image of the coupling between the BNA and the PC structure that is deduced from (a), (b) and Figure 2(e). Four regions are represented. In blue, the BNA transmits no power into the tip despite the laser is working: the BNA immersed in the near-field of the PC cavity is not resonantly excited because of polarization selectivity. In red, the laser is working and the BNA transmits power to the tip: the BNA is resonantly excited. In yellow, the BNA receives no power because the laser is quenched. In white, the BNA receives no power despite the PC structure is lasing because the BNA is not coupled to the near-field of the cavity.

The near-field images displayed in Figure 4(a) and (b) show identical distributions of dark spots which correspond to laser quenching since the detected signals fall down to zero in both images. Note that the diffraction pattern associated to the distribution of dark spots in Figure 4(b) is due to the back-diffusion of the laser emission by the tip apex. The dark regions common to Figure 4(a) and (b) are represented in yellow in the color-coded map of the BNA-to-PC optical coupling shown in Figure 4(c). They are located at the center of red patterns representing the areas over which the BNA is resonantly excited by the laser mode: the laser is working and the BNA, oriented along the local polarization direction of the cavity mode, transmits power into the tip. When the BNA is oriented perpendicularly to the local polarization of the cavity mode (cf. the blue areas shown in Figure 4(c)), it is not resonantly excited and the losses are much smaller as they do not trigger laser extinction. The polarization-dependent optical loss revealed here unambiguously proves that the funneling mechanism toward the BNA is due to the excitation of its resonant capacitive effect. Given the resonance properties of the BNA shown in Figure 1, we see that the loss channel is spatially localized right at the tiny feed gap of the BNA, over an area of about $0.0025\lambda^2$.

The fraction *F* of the laser power that is funneled into the nanometer scale feed gap of the BNA, i.e. the BNA coupling efficiency, can be deduced from the estimation of the losses of the PC cavity coupled to the BNA-on-tip. One possible way to address this issue is to measure the quality factor of the PC cavity in the presence of the BNA-on-tip. Q-factors are defined as $Q = \omega W/\phi$, where ω is the resonance frequency, *W* the energy stored within the resonator and ϕ the power losses.

We assume in the following that the overall losses of the hybrid system, and thus the ratio between the PC and the nano-antenna losses, are independent of the coupling conditions between the gain medium and the PC nanocavity. This condition implies that the direct coupling of the gain medium with the environment outside the PC laser nanocavity (ie. free-space and nano-antenna) can be neglected. Such

an assumption is here possible because the quantum wells are broadband emitters (the emission spectrum spreads over more than 200 nm) and show therefore low sensitivity to external perturbations. Moreover, quantum wells are embedded in a high refraction index InP layer which strongly confine the photons emitted by the gain medium within the nanocavity and thus limit the direct coupling of the quantum wells with the outside. Therefore, the overall loss ϕ_{tot} which results from the coupling of the PC laser to the BNA-on-tip can be written as the sum of the power losses of the PC laser nanocavity directly in free space and due to the coupling with the BNA-on-tip. Following the procedure shown previously, one can estimate the losses (ϕ_{BNA}) induced by the resonant excitation of the capacitive effect at the BNA feed gap by subtracting the loss values achieved when the BNA is on and off-resonance. The fraction F of the overall power that is funneled into the BNA takes then the simple form:

$$F = \frac{\phi_{BNA}}{\phi_{tot}} = 1 - \frac{Q_1}{Q_2} \qquad (1)$$

where Q_1 and Q_2 are the Q-factors of the hybrid structure when the BNA is resonantly and non-resonantly excited, respectively. Q_1 and Q_2 are obtained for the same position of the BNA-on-tip with respect to the nanocavity.

Figure 5: Resonance spectra of the PC laser nanocavity just below the laser emission threshold, when the cavity is free (red curve) and when the BNA-on-tip is placed at a distance of 145 nm from the PC surface, with its polarization axis parallel (blue curve, BNA non-resonant) and perpendicular (green curve, BNA resonant) to the cavity long axis (see insets).

To estimate the Q_1 and Q_2 values, we measured the linewidth of the resonances in the photoluminescence (PL) regime around threshold. Figure 5 shows the emission spectra of the PC structure measured just below laser threshold, close to the transparency regime of the gain medium, when the cavity is free and when it is coupled to the BNA-on-tip. First, the *L-L* curve (light-in versus light-out) is plotted for the free cavity to estimate the threshold pump power (extrapolation back of the *L-L* curve from above threshold) and a PL spectrum is measured just below laser threshold, in the transparency regime of the gain medium (red curve) [35]. Note that the pump beam area right at the microlaser is large enough to ensure that the entire cavity is pumped and thus non absorbing. The cold cavity Q-factor is then estimated to a value of $Q_0 = 3540 \pm 100$. Then, the BNA-on-tip is positioned at the center of the cavity and the BNA's polarization axis is set perpendicular to the cavity long axis (ie. the BNA is on-resonance). The BNA is placed at 145 nm away from the cavity surface, so that the hybrid structure operates just below the threshold with the maximum pump power (see the green curve of Figure 5). The Q-factor of the hybrid structure at the transparency regime of the gain medium is then estimated to $Q1 = 883 \pm 34$. Finally, the cavity and the pump polarization direction are turned by 90°, and the BNA-on-tip is placed at the same position with respect to the cavity, so that the BNA becomes non resonantly excited by the cavity mode. Because laser emission occurs in this configuration (involving maximum pump power), the pump level is reduced to reach PL emission just below threshold (see the blue curve of Figure 5). The Q-factor of the resulting hybrid structure at the transparency regime of the gain medium is then estimated to $Q_2 = 1095 \pm 45$. Note that spacing variations of a few nanometers between the tip and the cavity can have noticeable influence onto the resonance of the overall hybrid structure. Therefore, the spectrum acquisition time in the presence of the BNA-on-tip has been reduced to ensure that only negligible residual variation of the spacing between the two structures occurs during spectrum measurements. This explains why the signal-to-noise ratio of the spectra acquired in the presence of the BNA-on-tip (green and blue curves of Figure 5) is lower than in the case of the free cavity (red curve of Figure 5).

From the Q-factor measurements and Eq. (1), we find that at a spacing Z of about 145 nm, 19.4 ± 8.1% of the total optical power produced by the microlaser is transferred to the resonant capacitive effect of the BNA whose area is of $0.0025\lambda^2$, which is 1500 fold tighter than the overall emission area of the PC

microlaser. This power transfer to the BNA is here 79.2 times larger than the ratio between the overall area of the BNA and the total emission area of the PC laser nanocavity, which demonstrate the optical funneling phenomenon from the microlaser into the nano-antenna. Eq. (1) shows however that an increase of light coupling into the nano-antenna is irremediably linked to the broadening of the laser linewidth (ie. an increase of Q_2/Q_1). Therefore, the production of a laser nanosource in our case requires a trade-off between energy funneling toward the BNA and the preservation of the laser linewidth.

CONCLUSION

In conclusion, we have shown experimentally an optical funneling phenomenon from a diffraction-limited laser emission toward the nanometer-scale resonant mode of a BNA. The resulting energy transfer down to the nanoscale opens promising avenues in the light enhancement and confinement beyond the diffraction limit. This light funneling, demonstrated here with a BNA, may be reached with all other kinds of nano-antennas that show similar resonance properties in terms of emission wavelength and Q-factor, such as bowtie or dipole nano-antennas, dimers and single plasmonic nanoparticles. Therefore, it may provide an interesting alternative to the conventional nano-antenna addressing directly with far-field diffraction-limited focused waves which remains so far the main solution to deliver light down to a nano-antenna, but suffers from a lack of efficiency and compactness. The direct coupling of a nano-antenna to a PC laser nanocavity offers the possibility to efficiently address the nano-antenna in a compact optical architecture which does not exceed a few cubic microns. Nano-antennas may have also the intriguing ability to finely tune the emission wavelength, spectral linewidth and threshold of a microlaser (as shown here with the BNA) and may also control its emission properties [36].

ACKNOWLEDGEMENT

The authors are indebted to Remo Giust and Maria Garcia-Parajo for helpful discussions and revisions of the manuscript. This work is supported by the "Pôle de compétitivité Microtechnique", the Labex ACTION, and the french network of technology platforms "Renatech". It is funded by the "Agence Nationale de la Recherche" under contract number ANR07-NANO-036.

REFERENCES

[1] Novotny L, van Hulst N. Antennas for light. Nat. Photon. 2011; **5**: 83–90.
[2] Mühlschlegel P, Eisler HJ, Martin OJF, Hecht B, Pohl DW. Resonnant optical antenna. Science. 2005; **308:** 1607–1609.
[3] Aizpurua J, Bryant GW, Richter LJ, De Abajo FG, Kelley BK, Mallouk T. Optical properties of coupled metallic nanorods for field-enhanced spectroscopy. Physical Review B. 2005; **71** :235420.
[4] Grober RD, Schoelkopf RJ, Prober DE. Optical antenna : Towards a unity efficiency near-field optical probe. Appl Phys Lett. 1997: **70**: 1354–6.
[5] Schuck PJ, Fromm DP, Sundaramurthy A, Kino GS, Moerner WE. Improving the mismatch between light and nanoscale objects with gold bowtie nanoantennas. Phys. Rev Lett. 2005; **94**: 017402.
[6] Alù A, Engheta N. Hertzian plasmonic nanodimer as an efficient optical nanoantenna. Phys Rev B. 2008; **78**: 195111.
[7] Muskens OL, Giannini V, Sánchez-Gil JA, Rivas JG. Optical scattering resonances of single and coupled dimer plasmonic nanoantennas. Opt Express. 2007; **15**: 17736–17746.
[8] Wang L, Uppuluri S, Jin E, Xu X. Nanolithography using high transmission nanoscale bowtie apertures. Nano Lett. 2006; **6**: 361.
[9] Farahani JN, Pohl DW, Eisler HJ, Hecht B. Single quantum dot coupled to a scanning optical antenna : A tunable superemitter. Phys Rev Lett. 2005; **95**: 017402.1–4.
[10] Kinkhabwala A, Yu Z, Fan S, Avlasevich Y, Mullen K, Moerner WE. Large single-molecule fluorescence enhancements produced by a bowtie nanoantenna. Nat Photon. 2009; **3**: 654–657.
[11] Punj D, Mivelle M, Moparthi SB, van Zanten TS, Rigneault H, van Hulst NF, et al. A plasmonic/antenna-in-box/'platform for enhanced single molecule analysis at micromolar concentrations. Nat. Nanotechnol. 2013; **8**:512–516
[12] Fromm D, Sundaramurthy A, Kinkhabwala A, Schuck PJ, Kino G, Moerner W. Exploring the chemical

enhancement for surface-enhanced Raman scattering with Au bowtie nanoantennas. J Chem Phys. 2006; **124**: 061101.
[13] Hatab NA, Hsueh CH, Gaddis AL, Retterer ST, Li JH, Eres G, et al. Free-standing optical gold bowtie nanoantenna with variable gap size for enhanced Raman spectroscopy. Nano lett. 2010; **10**: 4952–4955.
[14] Hanke T, Krauss G, Träutlein D, Wild B, Bratschitsch R, Leitenstorfer A. Efficient Nonlinear Light Emission of Single Gold Optical Antennas Driven by Few-Cycle Near-Infrared Pulses. Phys. Rev. Lett. 2009; **103**: 257404.
[15] Righini M, Ghenuche P, Cherukulappurath S, Myroshnychenko V, de Abajo FJG, Quidant R. Nano-optical trapping of Rayleigh particles and Escherichia coli bacteria with resonant optical antennas. Nano Lett. 2009; **9**: 3387–3391.
[16] Cubukcu E, Kort EA, Crozier KB, Capasso F. Plasmonic laser antenna. Appl Phys Lett. 2006; **89**: 093120.
[17] Painter O, Lee R, Scherer A, Yariv A, O'Brien J, Dapkus P, et al. Two-Dimensional Photonic Band-Gap Defect Mode Laser. Science 1999; **284**: 1819–1821.
[18] Park HG, Kim SH, Kwon SH, Ju YG, Yang JK, Baek JH, et al. Electrically driven single-cell photonic crystal laser. Science. 2004; **305**: 1444–1447.
[19] Altug H, Dirk Englund JV. Ultrafast photonic crystal nanocavity laser. Nat. Physics. 2006; **2**: 484–488.
[20] Loncar M, Scherer A, Qiu Y. Photonic crystal laser sources for chemical detection. Appl. Phys. Lett. 2003; **82**: 4648-4650
[21] Barth M, Schietinger S, Fischer S, Becker J, Nusse N, Aichele T, et al. Nanoassembled plasmonic-photonic hybrid cavity for tailored light-matter coupling. Nano lett. 2010; **10**: 891–895.
[22] De Angelis F, Patrini M, Das G, Maksymov I, Galli M, Businaro L, et al. A Hybrid Plasmonic- Photonic Nanodevice for Label-Free Detection of a Few Molecules. Nano lett. 2008; **8**: 2321–2327.
[23] De Angelis F, Zaccaria RP, Francardi M, Liberale C, Di Fabrizio E. Multi-scheme approach for efficient surface plasmon polariton generation in metallic conical tips on AFM-based cantilevers. Opt. Express. 2011; **19**: 22268–22279.
[24] Belarouci A, Benyattou T, Letartre X, Viktorovitch P. 3D light harnessing based on coupling engineering between 1D-2D Photonic Crystal membranes and metallic nano-antenna. Opt. Express. 2010; **18**: 381–394.
[25] Jin EX, Xu X. Obtaining super resolution light spot using surface plasmon assisted sharp ridge nanoaperture. Appl. Phys. Lett. 2005; **86**: 111106–111106.
[26] Mivelle M, Ibrahim IA, Baida F, Burr GW, Nedeljkovic D, Charraut D, et al. Bowtie nano-aperture as interface between near-fields and a single-mode fiber. Opt Express. 2010; **18**: 15964–15974.
[27] Bachelot R, Ecoffet C, Deloeil D, Royer P, Lougnot DJ. Integration of Micrometer-Sized Polymer Elements at the End of Optical Fibers by Free-Radical Photopolymerization. Appl Opt. 2001; **40**:5860–5871.
[28] Taflove A, Hagness SC. Computational Electrodynamics : The Finite-Difference Time-Domain Method, Third Edition. Boston : Artech House; 2005.
[29] Huang JS, Kern J, Geisler P, Weinmann P, Kamp M, Forchel A, et al. Mode imaging and selection in strongly coupled nanoantennas. Nano Lett, 2010; 10: 2105-2110.
[30] Mivelle M, van Zanten TS, Neumann L, van Hulst NF, Garcia-Parajo MF. Ultrabright Bowtie Nanoaperture Antenna Probes Studied by Single Molecule Fluorescence. Nano letters. 2012 ; **12** :5972–5978.
[31] Guo R, Kinzel EC, Li Y, Uppuluri SM, Raman A, Xu X. Three-dimensional mapping of optical near field of a nanoscale bowtie antenna. Opt Express 2010; **18**: 4961–4971.
[32] Le Gac G, Rahmani A, Seassal C, Picard E, Hadji E, Callard S. Tuning of an active photonic crystal cavity by an hybrid silica/silicon near-field probe. Opt. Express. 2009; **17**: 21672–21679.
[33] Vo TP, Mivelle M, Callard S, Rahmani A, Baida F, Charraut D, et al. Nearfield probing of slow Bloch modes on photonic crystals with a nanoantenna. Opt. Express. 2012 ; **20**: 4124–4135.
[34] Grosjean T, El Eter A, Mivelle M, Vo TP, Belkhir A, Ecoffey C, et al. Extraordinary blueshift of a photonic crystal nanocavity by reducing its mode volume with an opaque microtip. Appl. Phys. Lett. 2012; **101**: 051102.
[35] Srinivasan K, Barclay PE, Painter O, Chen J, Cho AY, Gmachl C. Experimental demonstration of a high quality factor photonic crystal microcavity. Appl. Phys. Lett. 2003; **83**: 1915–1917.
[36] Yu N, Blanchard R, Fan J, Wang QJ, PflRgl C, Diehl L, et al. Quantum cascade lasers with integrated plasmonic antenna-array collimators. Opt. Express. 2008; **16**:19447–19461.

LIST OF FIGURES

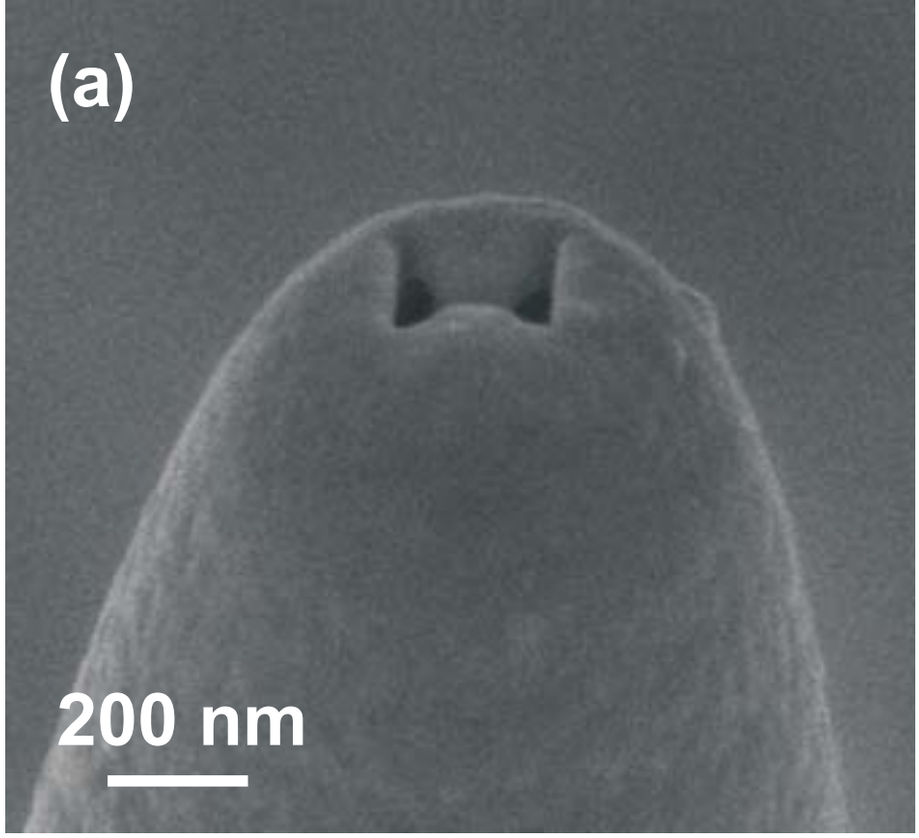
(a)
200 nm

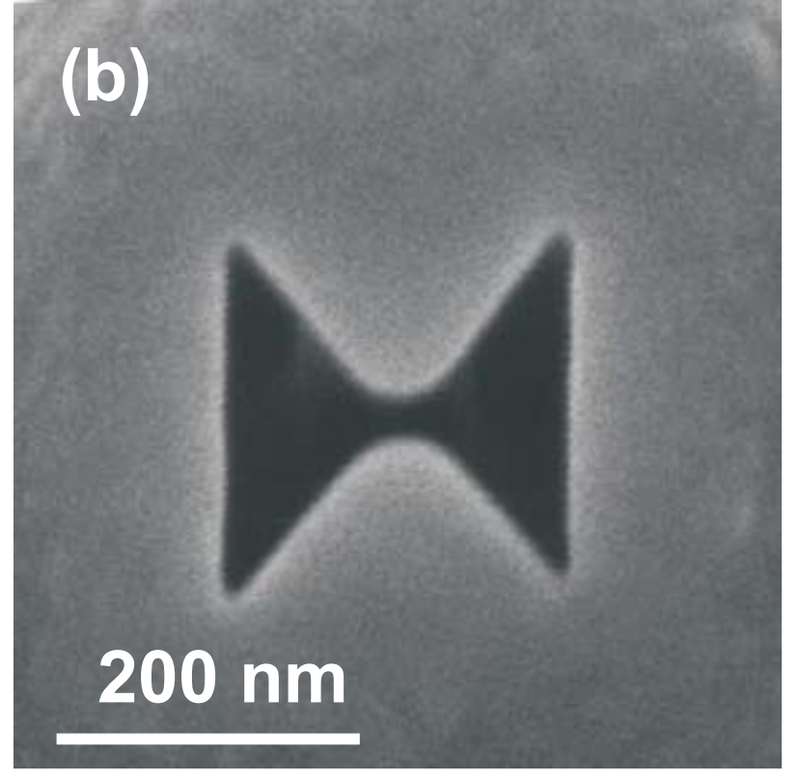
(b)
200 nm

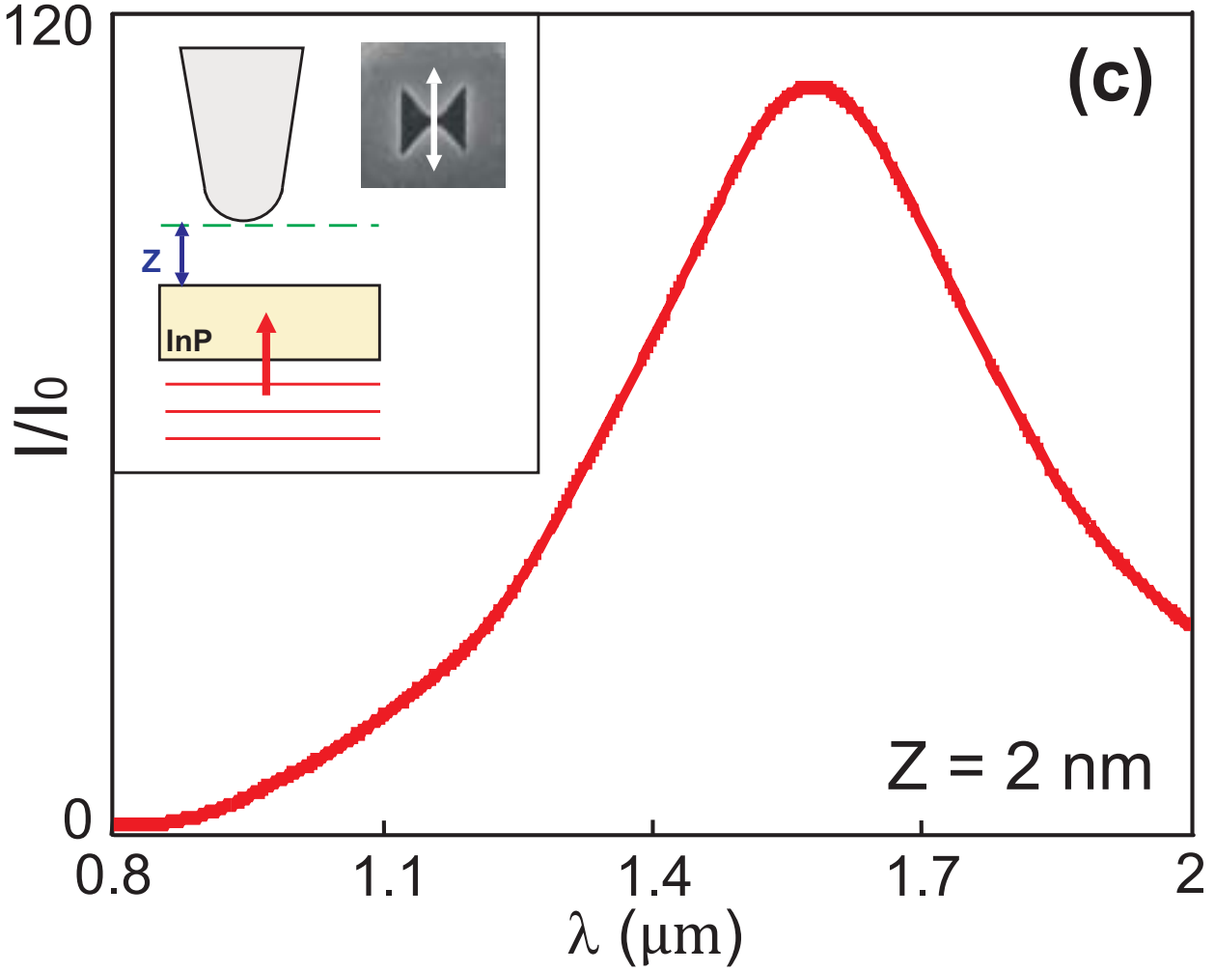
(c)
120
0
I/I0
z
InP
Z = 2 nm
0.8
1.1
1.4
1.7
2
λ (μm)

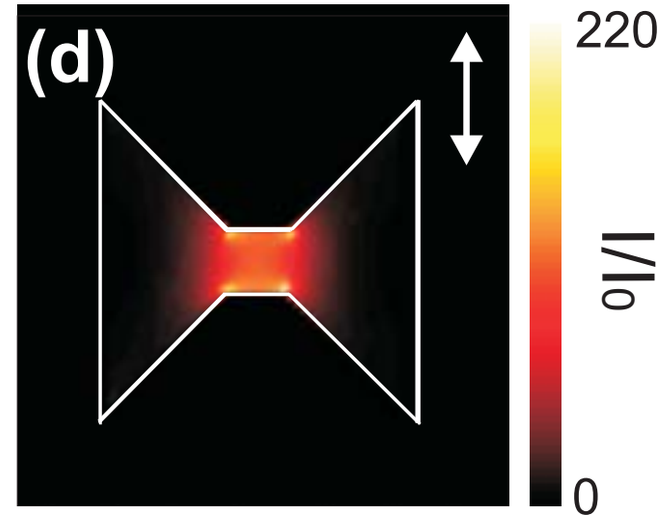
(d)
220
I/I0
0

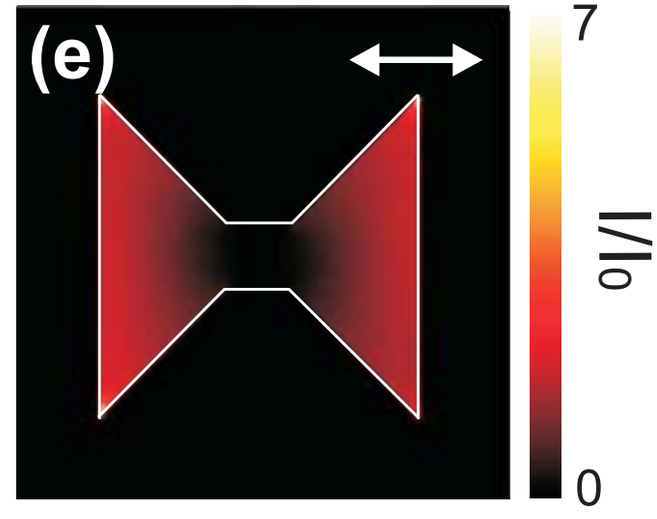
(e)
7
I/I0
0

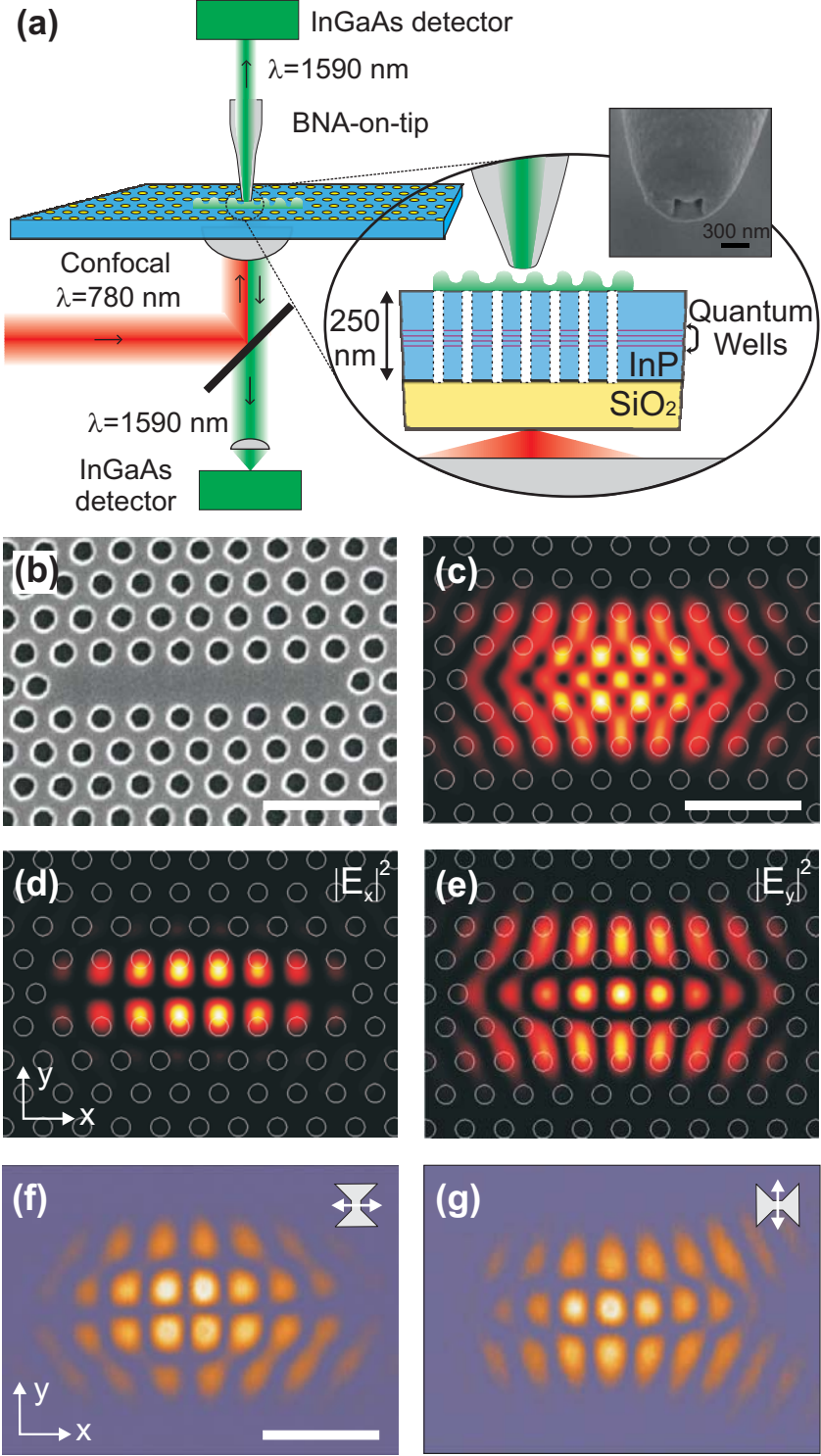
(a)
InGaAs detector
λ=1590 nm
BNA-on-tip
300 nm
Confocal
λ=780 nm
250
nm
Quantum
Wells
InP
SiO2
λ=1590 nm
InGaAs
detector
(b)
(c)
(d)
|Ex|2
y
x
(e)
|Ey|2
(f)
y
x
(g)

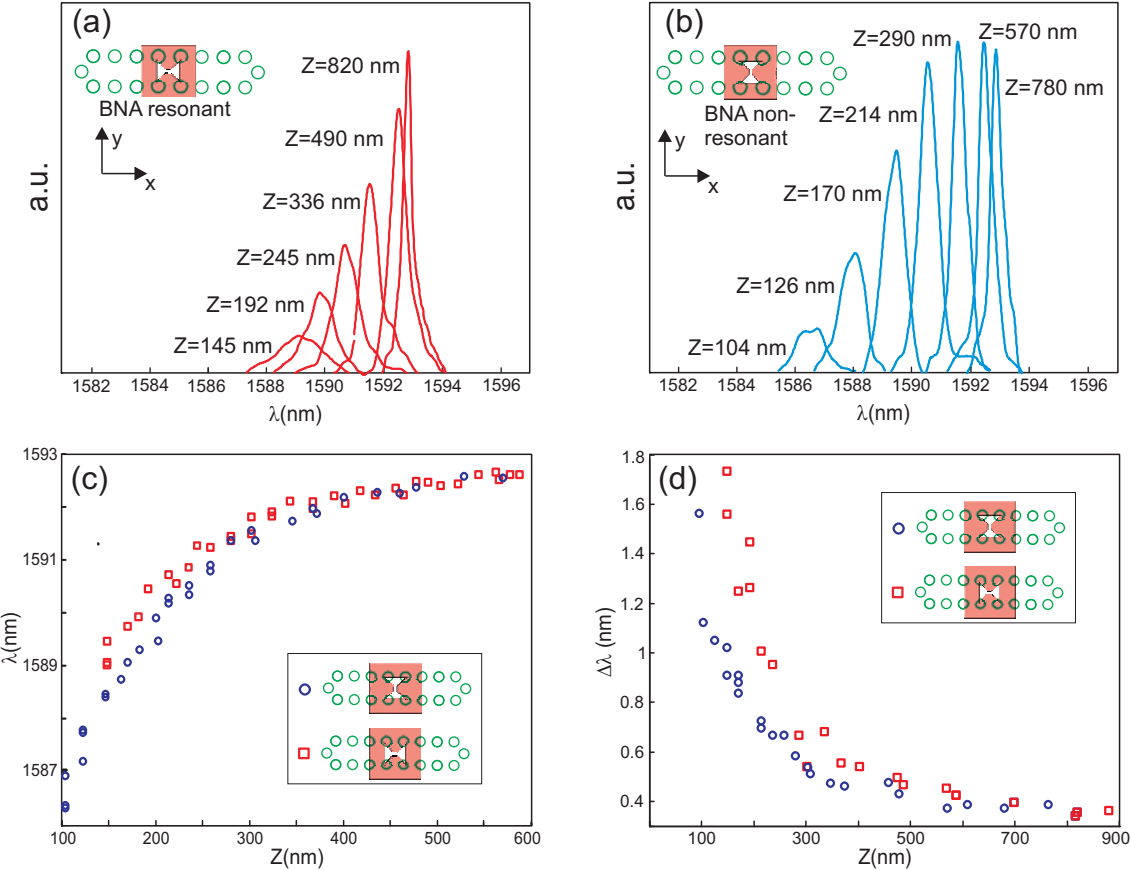
(a)
BNA resonant
y
x
Z=820 nm
Z=490 nm
Z=336 nm
Z=245 nm
Z=192 nm
Z=145 nm
a.u.
1582 1584 1586 1588 1590 1592 1594 1596
λ(nm)
(b)
BNA non-resonant
y
x
Z=290 nm
Z=570 nm
Z=780 nm
Z=214 nm
Z=170 nm
Z=126 nm
Z=104 nm
a.u.
1582 1584 1586 1588 1590 1592 1594 1596
λ(nm)
(c)
λ(nm)
1593
1591
1589
1587
100 200 300 400 500 600
Z(nm)
(d)
Δλ (nm)
1.8
1.6
1.4
1.2
1
0.8
0.6
0.4
100 300 500 700 900
Z(nm)

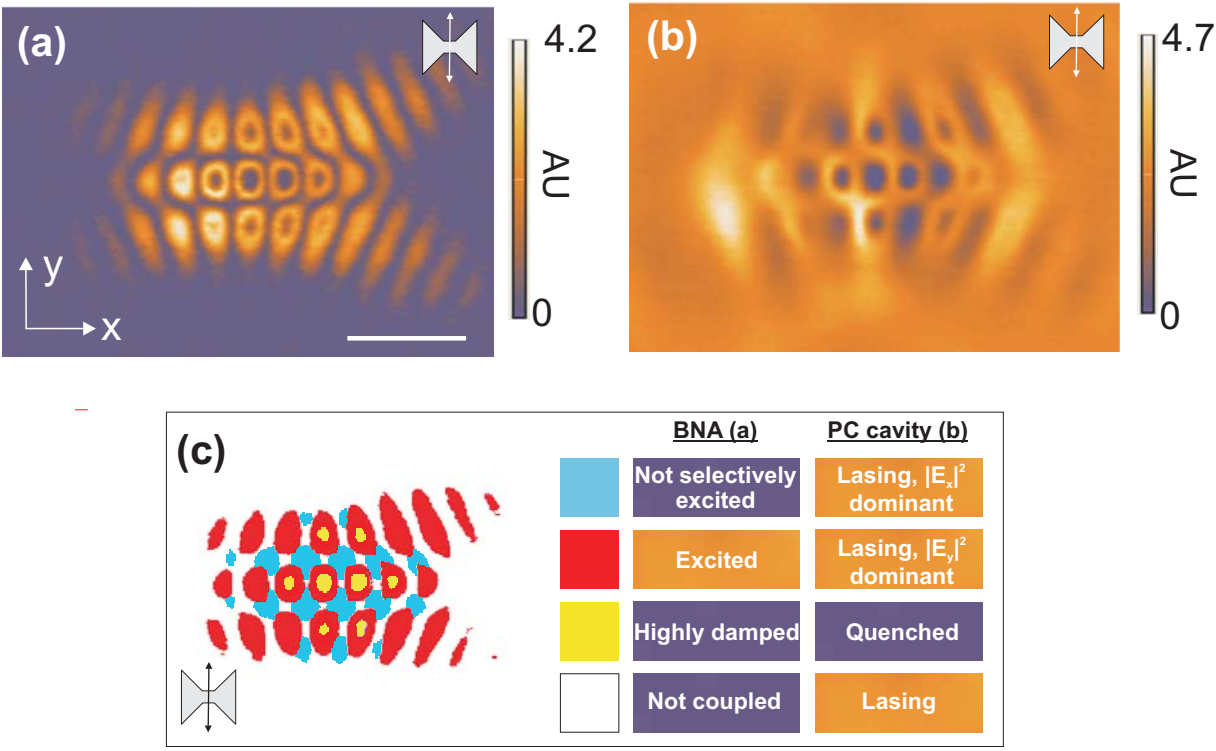
(a)
4.2
AU
0
y
x
(b)
4.7
AU
0
(c)
BNA (a)
PC cavity (b)
Not selectively excited
Lasing, $|E_x|^2$ dominant
Excited
Lasing, $|E_y|^2$ dominant
Highly damped
Quenched
Not coupled
Lasing

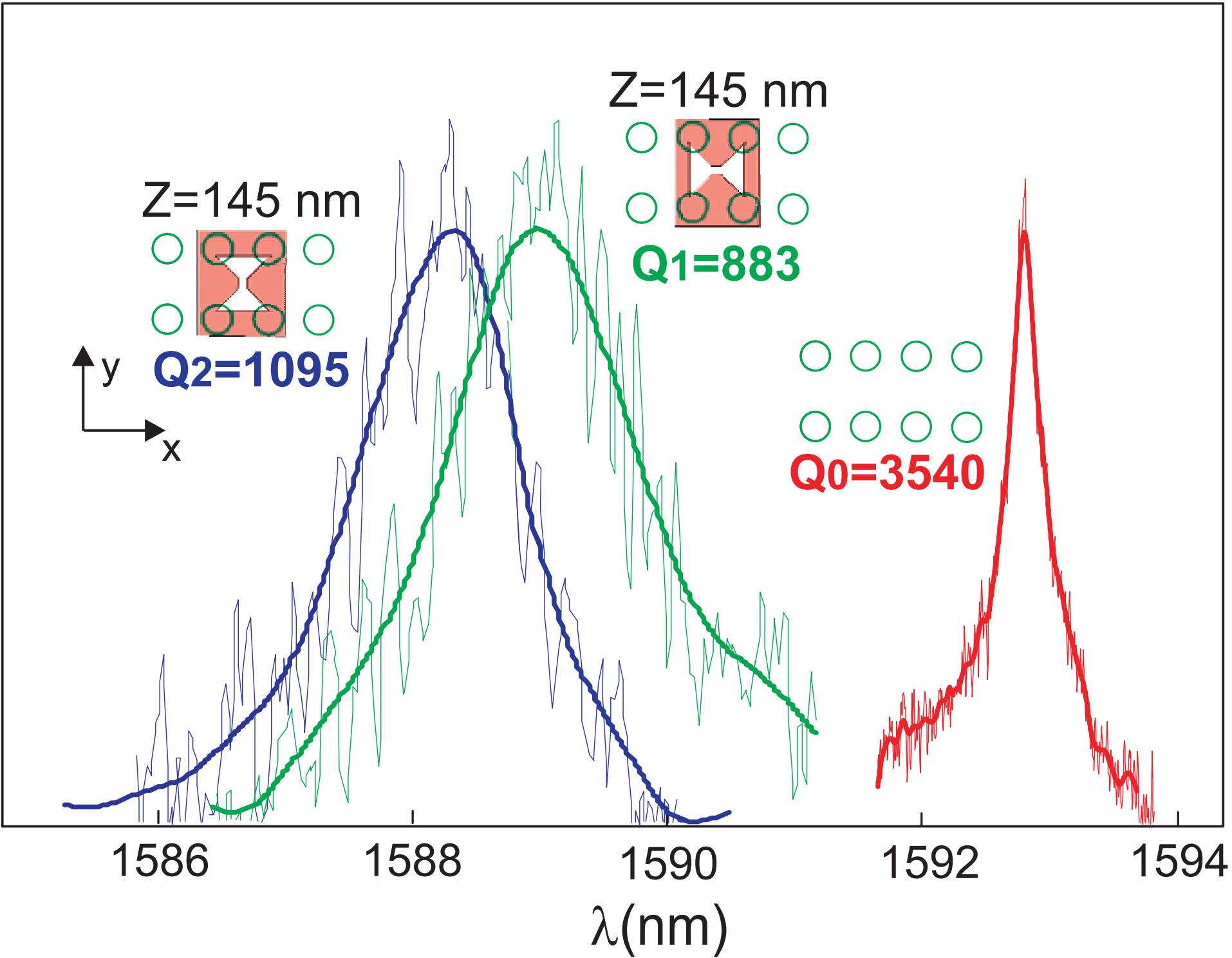
Z=145 nm
Z=145 nm
Q1=883
Q2=1095
Q0=3540
y
x
1586
1588
1590
1592
1594
λ(nm)